Square-shaped RNA particles from different RNA folds. Nano Lett

ARTICLE *in* NANO LETTERS · MARCH 2009

Impact Factor: 13.59 · DOI: 10.1021/nl900261h · Source: PubMed

Published in final edited form as:
Nano Lett. 2009 March ; 9(3): 1270–1277. doi:10.1021/nl900261h.

Square-Shaped RNA Particles From Different RNA Folds

Isil Severcan[1,+], **Cody Geary**[1,+], **Erik Verzemnieks**[1,2], **Arkadiusz Chworos**[1,3], and **Luc Jaeger**[1,*]

1 *Department of Chemistry and Biochemistry, University of California at Santa Barbara, Santa Barbara, CA 93106-9510*

Abstract

The structural information encoding specific conformations of natural RNAs can be implemented within artificial RNA sequences to control both three-dimensional (3D) shape and self-assembling interfaces for nanotechnology and synthetic biology applications. We have identified three natural RNA motifs known to direct helical topology into approximately 90° bends: a five-way tRNA junction, a three-way junction and a two-helix bend. These three motifs, embedded within rationally designed RNAs (tectoRNA), were chosen for generating square-shaped tetrameric RNA nanoparticles (NPs). The ability of each motif to direct the formation of supramolecular assemblies was compared by both native gel assays and atomic force microscopy (AFM). While there are multiple structural solutions for building square-shaped RNA particles, differences in the thermodynamics and molecular dynamics of the 90°-motif can lead to different biophysical behaviors for the resulting supramolecular complexes. We demonstrate via structural assembly programming how the different 90°-motifs can preferentially direct the formation of either 2D or 3D assemblies.

Introduction

The folding of RNA into compact 3D structures is a hierarchical process in which the formation of A-form helices is followed by the formation of tertiary motifs that specify the positioning of the helices within the structure[1, 2]. Due to the folding process of RNA, modular tertiary motifs have likely emerged for the purpose of adopting specific topological arrangements of helices[3–5]. RNA motifs are defined by sequence signatures that correspond to limited sets of conserved and semi-conserved nucleotides specifying well-defined 3D conformers[4–6]. Recent developments in RNA architectonics[7–11], an approach for rationally designing 3D RNA architectures, have established that RNA structure information can be implemented into an artificial sequence to direct its tertiary folding and supra-molecular assembly with a high degree of control and predictability. Nevertheless, knowledge about the kinetics, thermodynamics and autonomous folding properties of most RNA tertiary motifs remain scarce, presently limiting their use as building blocks for nano-construction. Three different 90°-motifs identified within RNAs from the translational apparatus have been examined for their ability to promote the assembly of square-shaped RNA nanoparticles (NPs). The right-angle motif (RA-motif), three-way junction motif (3WJ-motif) and tRNA-motif, which all have different local folds, contribute to forming 90° bend structures that could be seen as topologically equivalent (Fig. 1).

*To whom correspondence should be addressed: Phone: 805-893-3628; Fax: 805-893-4120; Email; jaeger@chem.ucsb.edu.
[2]Present address: School of Medicine, University of Washington, Seattle, WA 98125
[3]Present address: Department of Physics, UCSB, Santa Barbara, CA 93106.
[+]These authors contributed equally to this work

Supporting Information Available: File (Supporting_info.pdf) with extended Materials and Methods section and additional figures S1 to S9.

The RA-motif is a prevalent conserved structural motif found in ribosomal RNAs (Zhuang, Jaeger, unpublished data). It arranges adjacent helices similar to the corners of a log cabin, promoting packing of two helical stems along their shallow-grooves through ribose-zipper interactions[12]. It has been demonstrated that this motif is able to guide the assembly of L-shaped tectoRNAs into tetramers[8]. The 3WJ–motif, also called UA_h_3WJ[5], forms T-shaped arrangements of three helices (e.g. H75-H76-H79 in *H. marismortui* 23S rRNA), where the coaxial stacking of two helices is enforced and the third stem protrudes at a roughly 90° angle[5, 13]. Lastly, the tRNA-motif consists of a four to five helical junction that folds into an L-shape tertiary structure stabilized by conserved T-D loop and triple helix interactions[14].

While these motifs are topologically equivalent as 90° angles, differences in their thermodynamics, kinetics and other biophysical properties are likely to result from their different functions within their natural context. However, if the motifs are truly topologically equivalent they should be interchangeable irrespective of their functional differences. Here, we report on the design and characterization of square-shaped RNA NPs using these three different 90°-motifs as a means to compare the effect of different RNA folds within a similar structural context (Fig. 1). Of these RNA NPs, the design utilizing the tRNA 90°-motif was found to be significantly more thermostable than the previously described tectosquare particle based on the RA-motif [8]. This work provides means to generate rationally designed RNA NPs with tunable thermodynamic and self-assembly properties for controlling the formation of 2D and 3D architectures. Additionally, modular RNA NPs could have potential as scaffoldings for the delivery of RNA-based therapeutic molecules.

Results

Rational design of square-shaped particles

The three different 90°-motifs were used as structural cores for designing L-shaped tectoRNAs able to assemble into square-shaped tetramers (tectosquares) (Fig. 1). The design strategy was similar to the one previously used to construct RA-squares[8]. Each 90°-motif specifies for the tectoRNA corner. Further supramolecular assembly is promoted by two kissing loops (KL) that are covalently joined to this corner by two helical stems. A set of four different selective KL interactions (Fig. S1) leads to highly specific and addressable tectoRNA assembly into three different tectosquares (Fig. 1) of similar dimension, ranging from 12 to 14 nm on a side: the minor size variation results from ring-closure constraints imposed by the 3D structure of the different 90°-motifs. The 3WJ-motif sequence signature was used to design two tectoRNAs: one is displayed Figure 1B and the other (3WJ-P) contains the 3WJ-motif rotated 90° anticlockwise. Additional concerns needed to be addressed for constructing the tRNA-square due to its greater structural complexity compared to the other motifs (Fig. S2C). We chose a class II tRNA fold in order to circularly permutate the sequence of the molecule (Fig. S2C). This allowed relocation of the 5′/3′ termini from the aminoacyl stem to the variable stem, and insertion of KL motifs at the ends of extended aminoacyl and anticodon stems (Fig. 1). The tRNA-motif sequence was derived from the engineered $tRNA^{qser}$, a hybrid class I/class II tRNA known to fold into the correct tRNA tertiary structure without post-transcriptional modifications[14, 15]. As the proper folding of the class I $tRNA^{Phe}$ has been shown to be independent of the location of the 5′/3′ termini[16, 17], this suggests that the permutated $tRNA^{qser}$ should likewise fold properly.

Tectosquare self-assembly

Each tectosquare was assembled in a single annealing step by subjecting an equimolar mixture of four tectoRNAs to a denaturation-renaturation folding process (see Materials and Methods). At 0.2 mM Mg^{2+} and 4°C, most KL interactions used in this study (KL1-4) promote assembly with apparent equilibrium constants of dissociation (K_D) in the 10nM range (Fig. S1). These

KL interactions are therefore similar in stability and assemble at concentrations well below the usual working RNA concentration of 100 nM. Selective formation of tectosquares mediated by four different KL interactions (KL1-4) was confirmed by native PAGE analysis (Fig. 2B). The yield of correctly assembled tectosquares was estimated to be ~80% by PAGE.

Two primary factors contribute to the association of a closed square-shaped structure: a well-folded and rigid 90°-motif that stabilizes the square corners, and stable KL interactions that form the square sides. Therefore, depending on the structure, stability and rigidity of the 90°-motif and the thermodynamic stability of the KL interactions, tectoRNAs can be trapped into NPs of defined size. Previous studies of similar tectoRNAs lacking a 90°-motif yield octameric and dodecameric cyclic-structures[18]. By contrast, the three 90°-motif tectoRNAs in this study assemble primarily into tetramers (Fig. 2B), indicating that the bend motif significantly contributes to the formation of specific-sized NPs.

Self-complementary tectoRNA assembly

The contribution of each 90°-motif to the formation of closed NP multimers were examined using tectoRNAs designed with self-complemetary KLs (Fig. 2C). These tectoRNAs assemble end-to-end, either through KL1 or KL5 interactions (at 10°C and 0.2 mM Mg^{2+}, apparent Kd for KL1 and KL5 are 5.2 nM and 152 nM, respectively). Self-complementary tectoRNAs lacking a 90°-motif (but with 2D structure comparable to RA-tectoRNAs) were previously observed to assemble into a mixture of linear and cyclic multimers ranging from dimers to dodecamers and even larger assemblies[18]. By contrast, 90°-motif tectoRNAs with self-complementary KLs assemble under similar experimental conditions into small cyclic structures, mostly dimers, trimers or tetramers (Fig. 2C). 90°-motifs facilitate NP closure when compared to the multimers observed by Horiya et al, most likely because ring closure is entropically favored by bending the two tectoRNA arms. In presence of 15 mM Mg^{2+}, RA, 3WJ-P and tRNA tectoRNAs with KL1 form mostly dimers (Fig. 2C), indicating that the overall energy of the KL1 interactions is strong enough to considerably distort the structure of the three types of 90°-motif. In comparison, the thermodynamically weaker KL5 interaction shifts most tectoRNA constructs towards formation of cyclic trimers and tetramers (Fig. 2C). The observed differences in assembly patterns are dependent on the energy of the KL interactions between tectoRNA monomers, but are also related to the structural, dynamical and stability properties of their constitutive 90°-motif. For instance, the orientation of the 3WJ motif within the tectoRNA construct dramatically affects its assembly. The 3WJ-tectoRNA yields a fraction of tetramers for both KL1 and KL5, while the permutated 3WJ-P tectoRNA forms mostly dimers (Fig. 2C). The topological constraints of the 3WJ-motif likely create a preferential directionality of motion for bending the stems with respect of one another (Fig. S2D). Self-assembly into particular NPs is therefore dependent on the ability of tectoRNAs to bend. This effect is exemplified by the behavior of the tRNA-tectoRNAs, for which the topological constraints favor only formation of small closed–structures (Fig. S2D). In assemblies with the weaker KL5 interaction, a tRNA-tectoRNA with mutations in key nucleotide positions (C56->G, U55->G) known to destabilize the T/D loop interaction of the tRNA-motif (Fig. 2D) remains trapped into dimers, while the regular tRNA-tectoRNA forms mostly trimers (Fig. 2C). The T/D loop interaction in the tRNA-motif could behave as a topological energy barrier to slow the formation of kinetically trapped dimers, such that KL1 is energetic enough to overcome the barrier but KL5 is not.

Tectosquares thermal stability

The contribution of 90°-motifs to the thermal stability of assembled tectosquares was investigated by thermal gradient gel electrophoresis (TGGE), a method for separating different species based on a temperature-dependent conformational change[8, 19]. Apparent melting temperatures were determined for each tectosquare by measuring the decrease in the yield of

squares versus temperature (Fig. S3). At 15 mM Mg^{2+}, none of the three tectosquares disassemble within the range of temperature tested (Data not shown). By contrast at 0.2 mM Mg^{2+}, all TGGE profiles are typically characterized by two-phase transitions (Fig. S3A). The first transition corresponds to a decrease in the mobility of the tectosquares around 25°–33°C, and is likely due to transient opening of the tetramers at one of the KL interactions. The second transition corresponds to the dissociation of the tectosquares into monomers. The tRNA-square has an apparent Tm of 46°C, about 8–10°C higher than the Tm of the RA-and 3WJ-squares (Fig. S3B). Because all tectosquares have the same assembly interfaces, these results indicate that the tRNA-motif contributes more to the overall tectosquare thermal stability than the RA- and 3WJ-motifs. The melting process for all three tectosquares is highly cooperative as it occurs over a ~15°C range.

We previously demonstrated that tectosquares with the RA-motifs were more stable than those without any [8]. The thermal stability of the RA-square was shown to increase with an increasing number of RA-motifs present within its assembly. Accordingly, the same trend is also observed for tRNA-squares, strongly supporting the notion that the 90°-motif cooperatively contributes to the overall tectosquare stability and assembly. Mutated tRNA-squares were generated from tectoRNAs with specific mutations knocking out the T/D loop interaction of the tRNA-motif (Fig. 2D). A decrease in the square association yield is directly correlated with an increasing number of mutated motifs incorporated per tRNA-square (Fig. S4). The yield of assembly of the tRNA-square with four mutated tRNA-motifs is five times lower than for the regular tRNA-square. Additionally, thermal stability of the fully mutated tRNA-square was shown by TGGE to be ~6°C lower than the regular tRNA-square in presence of 0.2 mM Mg^{2+} (Fig. 2F). Interestingly, this is still 3 to 4°C above the stability of the RA and 3WJ-squares, suggesting that the structure of the mutated tRNA-motif is only partially disrupted and still contributes significantly to the overall stability of the mutated tRNA-square.

Structural Probing of tRNA-squares

To investigate the 3D structure of our most stable tectosquare, chemical and enzymatic probing were performed on purified regular and mutated tRNA squares in presence of 15 mM Mg^{2+} and 50 mM K^{+} (Figs. 2DE and S5). Pb^{2+} is known to induce specific cleavages at the level of a magnesium-binding pocket within the D-loop of tRNA native folds[20–22]. Comparison of the Pb^{2+}-cleavage patterns of regular and mutated tRNA-squares showed a significant reduction of specific Pb^{2+}-induced cleavages within the D-loop of the mutated tRNA-motif, evidence that the mutated tRNA-square does not form stable T/D-loop interactions (Fig. 2DE). Moreover, an increase in the accessibility of the T and D loops regions of the mutated tRNA-square was observed by cleavage with RNase T1, a ribonuclease known to specifically cleave in 3′ of single stranded Gs and As. Both results corroborate the direct involvement of the tRNA-motif on square stability. At the exception of the KL regions, there is no observed difference between Pb^{2+}-cleavage patterns of the motif as a monomer alone or within the tetramer, suggesting that the assembly of the tectoRNA unit into the tRNA-square structure does not alter the native fold of the tRNA motif (Fig. 2DE). However, T1 cleavage patterns reveal an increase in protection from digestion of the tRNA-square versus the monomer unit alone. Therefore, tertiary NP assembly can contribute to protecting RNA from ribonuclease degradation (Fig. S5A).

AFM structural analysis of squares

Further structural characterizations were performed by AFM to demonstrate that the RA, 3WJ and tRNA-squares are square-shaped assemblies. Tectosquares were assembled in solution and then deposited on a mica surface in 15 mM Mg^{2+} buffer, as reported previously[8, 23]. For all three tectosquares, AFM revealed uniform mono-dispersed particles with size and shape similar to the theoretical 3D models (Fig. 3). A central cavity is visible for each type of

tectosquare. The theoretical estimated size of the RA, 3WJ and tRNA-square models are 10 nm, 10 nm and 12 nm, (helix-center to center) respectively. Their average sizes were measured by AFM to be 12.0 ± 2.8, 9.0 ± 2.6 and 12.1 ± 2.3 nm respectively (Fig. 3C). Tectosquare heights were all measured to be ~1.5 nm, consistent with the previously observed height for a double helix of nucleic acid on a mica surface[8]. However, the corners of the tRNA-square appear to be bulkier in the images (Fig. 3A), which is consistent with the 3D model predicting the variable loop stem to be oriented out of the plane of the square (Fig. 1, side view).

The most prominent difference between the three tectosquares is their apparent yield on the surface. The adsorption ratios estimated from the number of NPs observed in a 1 μm^2 window, were calculated to be 12, 595 and 125 NP/μm^2 for RA, 3WJ and tRNA-squares, respectively (Fig. 3B). While RNA sample preparation (e.g. incubation time, washing process, buffer composition and AFM protocol) could potentially affect NPs adsorption process on mica, the same trend was observed when AFM imaging was performed in air or under 15mM Mg^{2+} solution. The resolution of AFM images of NPS obtained under solution was however not as good as the one obtained in air (data not shown). Since the yield of squares determined by PAGE is roughly equivalent between the three varieties, the difference in adsorption ratio of NPs on the mica surface is likely due to differences in the overall 3D shape of the NPs that result from the different structural and dynamical characteristics of the constituent 90°-motifs. For instance, the 3WJ-square that is the flattest of the tectosquares is also the one with the highest yield on the surface (Fig. 1, side view). In the case of the tRNA-squares, the variable stems, which can protrude approximately perpendicular to one side of tRNA-squares, likely decrease the ability of these tectosquares to bind mica on that side. Being a non-planar assembly (Fig. 1, side view), the RA-square has less potential surface contacts that explain its lower adsorption yield on mica. For instance, the shape/size of RA-squares could change when it interacts with mica surface, resulting in an observed rhombus/shape with measured dimensions (Fig. 3C) in slight discrepancy with the predicted dimensions of the square (Fig. 1A).

AFM structural analysis of tectosquare assemblies

While the three 90°-motifs are structurally equivalent for generating tectosquares, the way they control the directionality of the 3′ tail used for tail-tail assembly (Fig. 1 side view) will affect the way tectosquares assemble into more complex architectures. RNA arrays made of 3WJ- and tRNA-squares assembling via programmed tail-tail connectors were designed using the strategy previously reported for RA-square arrays[8] (Figs. S6 and S7). After assembly in solution and deposition on a mica surface in 15 mM Mg^{2+} buffer, the different tectosquares arrays were visualized by AFM as reported previously[8, 23]. An assembly system of two 3WJ-squares can form either a 1D ladder (Fig. 4A) or a 2D array (Fig. 4BC), depending the parallel or non-parallel arrangement of the units within the squares, respectively. The parallel arrangement is obtained by permutation of the KLs on units A and C (Fig. S6). As shown by AFM, the 3WJ-motif controls the precise coaxial stacking and directionality of the 3′ tail stems of the 3WJ-squares to form 1D and 2D planar arrays in a predictable way (Fig 4ABC).

Unlike the 3WJ-motif, the tRNA-motif has its 3′tail stem oriented out of the plane defined by the tRNA-square, preventing the design of tRNA-ladders with a parallel arrangement of units. For the tRNA-motif, a system of three squares and three different sets of tail-tail connector (each used twice) was used to program different assemblies (Figs. 4DEF and S7). With 2-2′, 3-3′, 4-4′ and 5-5′ connectors, tRNA-squares are shown by AFM to preferentially assemble into ladder-like dimers or trimers (Fig. 4D). Alternatively, when only 1-1′, 2-2′ and 3-3′ connectors are used, the tRNA-squares assemble preferentially into triangular-shaped triads (Fig. 4E). However, when all six connectors are present, rather than extending the ladder-like trimers into longer 1D ladders, the tRNA-squares generate compact discrete particles with an average height of 3.4 ± 0.7 nm (Figs. 4F and S8). These particles are at least two times taller

than regular tRNA-squares (Figs. S8). They are therefore likely to correspond to squished 3D tRNA-prisms due to the force applied by the AFM tip during imaging. The fact that these particles are closed tRNA-square particles is corroborated further by the observation that they migrate faster than the opened triads on native PAGE (Fig. S9). The yield of tRNA-prism formation was estimated by PAGE and AFM to be ~30–35%. The observed difference in assembly morphology that results from the use of different numbers of tail connectors to link a set of similar tRNA-squares suggests that the variable arm of the tRNA-motif is flexible. Notably, as the tRNA-square is the most stable tectosquare that we examined, the inherent flexibility of the variable arm does not appear to affect the tRNA-square stability but is rather an advantage for the nano-construction of 3D objects based on tRNA-squares.

Discussion

Artificial self-assembling RNAs can contribute to our understanding of the topological properties and structural dynamics of RNA motifs outside their natural context. Topologically equivalent 90°-motifs characterized by distinct local tertiary folds can lead to similar square-shaped RNA NPs. The tertiary structure of the three 90°-motifs used to assemble NPs impacts the flatness of the resulting particles, and consequently their property of adhesion on mineral surfaces. Furthermore, factors such as the thermodynamic stability and structural dynamics of a motif have a major effect on the resulting supramolecular assemblies composed of the motif. Therefore, an assortment of different RNA motif modules might provide the ability to tune the physical properties of RNA NPs for different technological applications.

We find that the thermodynamic stability of KL and tail-tail connectors can be large enough to overcome the fold of a 90°-motif if ring closure is possible. This effect is observed when self-complementary KL constructs assemble into cyclic dimers or trimers (Fig. 2C) rather than cyclic tetramers as suggested by the 3D computer modeling (Fig. 1). Molecular competition experiments suggest that the energy needed to overcome the folding of the RA-motif is only on the order of few kcal/mol (Zhuang, Shea and Jaeger, unpublished data), in agreement with the notion that the RA-motif is a rather dynamic bending motif. Once the RA-motif tectoRNA forms a dimer bridged by a single KL interaction, there is a propensity for the assembly to entropically close via the other KL-ends at a tradeoff of deforming the RA-motif (Fig. S2D). Furthermore, in an apparent interplay between structure and dynamics, the energy cost to deforming an RNA motif can vary depending on which direction the motif is bent. The dramatic difference in the behavior of the 3WJ and 3WJ-P motifs in ring-closure experiments (Fig. 2C) demonstrates that flexibility is not equally distributed between the three stems of the 3WJ-motif (Fig. S2D). While energetically strong KL interactions were able to distort the 3WJ-motif for ring-closure, comparatively weaker tail-tail interactions did not appear to distort the motif in array formation (Fig. 4C). For these reasons, the 3WJ-motif seems ideally suited for building branched 2D arrays.

The conformational dynamics of RNA tertiary motifs can be a useful feature in future rational designs, especially if the thermostability of the RNA is not compromised by the dynamics. For example, the tRNA-motif used in our study can be easily distorted from a 90°-angle to a 60°-angle and smaller (Figs. 1, 2BC), even though tRNA-squares have increased thermostability compared to the other tectosquares (Fig. S3). The thermostability of the tRNA-square, as well as its increased resistance towards ribonuclease digestion could be advantageous for future biomedical applications. Additionally, because objects built up from multiple tRNA-squares can be connected in numerous different ways due to the flexibility of the variable arm (Fig. 4DEF), the tRNA-motif can be a versatile building block for building different 3D architectures.

Conclusion

As shown herein, supramolecular self-assembly can be used to explore and compare the biophysical properties of RNA tertiary structure motifs that would otherwise be more difficult to investigate in isolation or within their natural context (see also[8, 24, 25]). Additionally, this strategy offers great potential in nanobiology and nanomedicine[10, 26, 27]. Structural RNA NPs can be used to combine multiple functionalities in one delivery particle for various therapeutic purposes[27]. For example, the natural pRNA molecule from the phi29 DNA-packing motor[11] was engineered to create multifunctional pRNA particles for delivery of siRNAs to cancer cells via specific targeting of CD4 receptors[28], or for targeted delivery of ribozymes against the hepatitis B virus[29]. The tectosquare NPs presented in this study are stable RNA scaffoldings that offer an alternative to the phi29 pRNA scaffolding. Their thermodynamic properties can be finely tuned based on the complexity of the structural motifs used to build the RNA. Moreover, the ability of RNA tertiary motifs to kinetically direct the assembly into a well-defined NP can be used to further expand the application of rationally designed RNA NPs.

We have demonstrated that RNA tertiary motifs can be used to design complex 3D objects such as the tRNA-prism. RNA offers the potential to build multimeric 3D objects that assemble through tertiary interfaces that do not have to rely on tensegrity. Likewise to a variety of self-assembling polygonal shapes (e.g. refs[30–32]) generated by DNA nano-construction[7, 33, 34], RNA 3D objects could be used as functional nanocontainers for therapeutic delivery[31]. We anticipate that self-assembling RNA NPs will contribute positively to the development of new biomedical applications in the future, especially because it can be more readily expressed in vivo than DNA[35].

Materials and Methods

TectoRNA design and synthesis

3D atomic models were manually constructed using Swiss-Pdb Viewer as previously described[7]. The RA-square model corresponds to the previous LT tectosquare model[8]. The 3WJ- and tRNA-squares were built likewise using 90° motifs extracted from the following x-ray structures: *E. Coli* 50S (2AW4) for the 3WJ motif, yeast $tRNA^{Phe}$ (4TNA) and *T. thermophilus* $tRNA^{Ser}$ (1SER) for the tRNA motif. The KL motif was extracted from the DIS HIV-1 kissing complex structure (IJJM). TectoRNAs were synthesized by in vitro T7 run-off transcription from PCR generate templates, purified by denaturing PAGE and 3′-[^{32}P]pCp labeled as previously described [24] (See Supporting Information (SI)).

Tectosquares Assembly

Tectosquares are prepared by mixing equimolar concentrations of four tectoRNAs (200 nM) in water. After denaturation (3 min, 90°C; 3 min, 4°C; 3 min, 30°C), samples were renatured in 10 mM Tris-borate pH 8.2 (TB), 50 mM KCl, and 0.2 mM $Mg(OAc)_2$ at 30°C for 30 mins. For AFM and native-PAGE, $Mg(OAc)_2$ concentration was typically raised to 15 mM and heated at 50°C for 10 min before cooling to 4°C. For visual monitoring on gels, 1 nM of tectosquare unit A is radiolabeled.

Native-PAGE and TGGE assays

Native 8% (29:1) PAGE and TGGE experiments were performed as previously described[8, 19, 24] (see SI). Apparent equilibrium constants of dissociation (K_D) for KL interactions were determined at 0.2 mM $Mg(OAc)_2$ as previously described[24] (see SI). K_D values correspond to the concentration at which half of the RNA molecules are dimerized. For TGGE analysis performed at 0.2 mM $Mg(OAc)_2$, a linear temperature gradient, typically from 25 °C to 65 °

C, was applied perpendicular to the electric field. Tectosquare concentration was typically of 40 nM. Thermal stability of the tRNA-square was not concentration dependent in the range of RNA concentrations tested (40–200 nM) (data not shown).

Lead-induced cleavage and RNase T1 structural probing

Probing of single tectoRNAs (400 nM) or tRNA-squares (100nM), purified on 8% native-PAGE prior probing, were done at 15mM Mg^{2+}. Pb^{2+} cleavage was performed as previously described[24, 25] (see SI). RNase T1 probing was performed according to the manufacturer recommendation (Ambion) (see SI). Pb^{2+} and RNase T1 cleavage patterns were visualized on denaturing 15% PAGE.

Atomic Force Microscopy (AFM)

20 μl tectosquare samples (100 nM RNA) were directly deposited on freshly cleaved mica surface for 60 sec, rinsed with a 2 mM $Mg(OAc)_2$ solution and dried with nitrogen. Imaging in air at ~20°C was performed in tapping mode on a Multimode AFM equipped with a Nanoscope IIIa controller (Veeco, Santa Barbara). AFM images of tectosquare 2D and 3D assemblies were obtained under solution as described[8]. Silicon probes (model NSC12 from MikroMesch) with resonance frequency ~150–250 kHz and spring constant ~4–8 N/m (Nanodevices, Santa Barbara, CA) were used. Images were processed by NanoScope® (DI) and leveled by a first order plane fit in order to correct the sample tilt.

Supplementary Material

Refer to Web version on PubMed Central for supplementary material.

Acknowledgements

LJ wishes to dedicate this paper to St. François de Sales and St. Jean-Baptiste de la Salle. Funding for this research was provided by NIH (R01 GM079604) and NSF (DMR 05-20415) to LJ. We thank Dr. Helen G. Hansma for the generous use of her AFM and laboratory facilities. We thank Dr. Irene Revenko (Asylum Research Inc.) for her help obtaining the AFM images in Figure 4BC.

References

1. Tinoco I Jr, Bustamante C. How RNA folds. J Mol Biol 1999;293(2):271–81. [PubMed: 10550208]
2. Woodson SA. Metal ions and RNA folding: a highly charged topic with a dynamic future. Curr Opin Chem Biol 2005;9(2):104–9. [PubMed: 15811793]
3. Hendrix DK, Brenner SE, Holbrook SR. RNA structural motifs: building blocks of a modular biomolecule. Q Rev Biophys 2005;38(3):221–43. [PubMed: 16817983]
4. Leontis NB, Lescoute A, Westhof E. The building blocks and motifs of RNA architecture. Curr Opin Struct Biol 2006;16(3):279–87. [PubMed: 16713707]
5. Jaeger L, Verzemnieks EJ, Geary C. The UA_handle: a versatile submotif in stable RNA architectures. Nucleic Acids Res 2009;37(1):215–30. [PubMed: 19036788]
6. Lescoute A, Leontis NB, Massire C, Westhof E. Recurrent structural RNA motifs, Isostericity Matrices and sequence alignments. Nucleic Acids Res 2005;33(8):2395–409. [PubMed: 15860776]
7. Jaeger L, Chworos A. The architectonics of programmable RNA and DNA nanostructures. Curr Opin Struct Biol 2006;16(4):531–43. [PubMed: 16843653]
8. Chworos A, Severcan I, Koyfman AY, Weinkam P, Oroudjev E, Hansma HG, Jaeger L. Building programmable jigsaw puzzles with RNA. Science 2004;306(5704):2068–72. [PubMed: 15604402]
9. Koyfman AY, Braun G, Magonov S, Chworos A, Reich NO, Jaeger L. Controlled spacing of cationic gold nanoparticles by nanocrown RNA. J Am Chem Soc 2005;127(34):11886–7. [PubMed: 16117496]
10. Yingling YG, Shapiro BA. Computational design of an RNA hexagonal nanoring and an RNA nanotube. Nano Lett 2007;7(8):2328–34. [PubMed: 17616164]

11. Shu D, Moll WD, Deng Z, Mao C, Guo P. Bottom-up Assembly of RNA Arrays and Superstructures as Potential Parts in Nanotechnology. Nano Lett 2004;4(9):1717–1723.
12. Gagnon MG, Steinberg SV. GU receptors of double helices mediate tRNA movement in the ribosome. RNA 2002;8(7):873–7. [PubMed: 12166642]
13. Lescoute A, Westhof E. Topology of three-way junctions in folded RNAs. Rna 2006;12(1):83–93. [PubMed: 16373494]
14. Nissan TA, Oliphant B, Perona JJ. An engineered class I transfer RNA with a class II tertiary fold. RNA 1999;5(3):434–45. [PubMed: 10094311]
15. Nissan TA, Perona JJ. Alternative designs for construction of the class II transfer RNA tertiary core. RNA 2000;6(11):1585–96. [PubMed: 11105758]
16. Pan T, Gutell RR, Uhlenbeck OC. Folding of circularly permuted transfer RNAs. Science 1991;254 (5036):1361–4. [PubMed: 1720569]
17. Pan T, Uhlenbeck OC. Circularly permuted DNA, RNA and proteins--a review. Gene 1993;125(2): 111–4. [PubMed: 7681803]
18. Horiya S, Li XG, Kawai G, Saito R, Katoh A, Kobayashi K, Harada K. RNA LEGO: Magnesium-dependent formation of specific RNA assemblies through kissing interactions. Chemistry & Biology 2003;10(7):645–654. [PubMed: 12890538]
19. Hartmann, RK.; Bindereif, A.; Schon, A.; Westhof, E. Handbook of RNA Biochemistry. Vol. 1. Wiley-VCH: Weinheim; 2005. p. 487
20. Werner C, Krebs B, Keith G, Dirheimer G. Specific cleavages of pure tRNAs by plumbous ions. Biochim Biophys Acta 1976;432(2):161–75. [PubMed: 773433]
21. Brown RS, Hingerty BE, Dewan JC, Klug A. Pb(II)-catalysed cleavage of the sugar-phosphate backbone of yeast tRNAPhe--implications for lead toxicity and self-splicing RNA. Nature 1983;303 (5917):543–6. [PubMed: 6343887]
22. Pan T, Uhlenbeck OC. A small metalloribozyme with a two-step mechanism. Nature 1992;358(6387): 560–3. [PubMed: 1501711]
23. Hansma HG, Oroudjev E, Baudrey S, Jaeger L. TectoRNA and 'kissing-loop' RNA: atomic force microscopy of self-assembling RNA structures. J Microsc 2003;212(Pt 3):273–9. [PubMed: 14629553]
24. Jaeger L, Westhof E, Leontis NB. TectoRNA: modular assembly units for the construction of RNA nano-objects. Nucleic Acids Res 2001;29(2):455–63. [PubMed: 11139616]
25. Geary C, Baudrey S, Jaeger L. Comprehensive features of natural and in vitro selected GNRA tetraloop-binding receptors. Nucleic Acids Res 2008;36(4):1138–52. [PubMed: 18158305]
26. Chworos, A.; Jaeger, L. Nucleic acid foldamers: design, engineering and selection of programmable bio-materials with recognition, catalytic and self-assembly properties. In: Hecht, SHI., editor. Foldamers: Structure, Properties, and Applications. Wiley-VCH: Weinheim; 2007. p. 291-330.
27. Severcan, I.; Geary, C.; Jaeger, L.; Bindewald, E.; Kasprzak, W.; Shapiro, BA. Computational and Experimental RNA Nanoparticle Design. In: Alterovitz, G.; Ramoni, M.; Mary Benson, R., editors. Automation in genomics and proteomics: An engineering case based approach. Wiley; New York: 2008. p. 193-220.
28. Khaled A, Guo S, Li F, Guo P. Controllable self-assembly of nanoparticles for specific delivery of multiple therapeutic molecules to cancer cells using RNA nanotechnology. Nano Lett 2005;5(9): 1797–808. [PubMed: 16159227]
29. Hoeprich S, Zhou Q, Guo S, Shu D, Qi G, Wang Y, Guo P. Bacterial virus phi29 pRNA as a hammerhead ribozyme escort to destroy hepatitis B virus. Gene Ther 2003;10(15):1258–67. [PubMed: 12858191]
30. Shih WM, Quispe JD, Joyce GF. A 1.7-kilobase single-stranded DNA that folds into a nanoscale octahedron. Nature 2004;427(6975):618–21. [PubMed: 14961116]
31. Goodman RP, Heilemann M, Doose S, Erben CM, Kapanidis AN, Turberfield AJ. Reconfigurable, braced, three-dimensional DNA nanostructures. Nat Nanotechnol 2008;3(2):93–6. [PubMed: 18654468]
32. He Y, Ye T, Su M, Zhang C, Ribbe AE, Jiang W, Mao C. Hierarchical self-assembly of DNA into symmetric supramolecular polyhedra. Nature 2008;452(7184):198–201. [PubMed: 18337818]

33. Seeman NC. An overview of structural DNA nanotechnology. Mol Biotechnol 2007;37(3):246–57. [PubMed: 17952671]

34. Aldaye FA, Palmer AL, Sleiman HF. Assembling materials with DNA as the guide. Science 2008;321 (5897):1795–9. [PubMed: 18818351]

35. Lin C, Rinker S, Wang X, Liu Y, Seeman NC, Yan H. In vivo cloning of artificial DNA nanostructures. Proc Natl Acad Sci U S A 2008;105(46):17626–31. [PubMed: 18927233]

36. DeLano, WL. The PyMOL Molecular Graphics System. DeLano Scientific; Palo Alto, CA, USA: 2002.

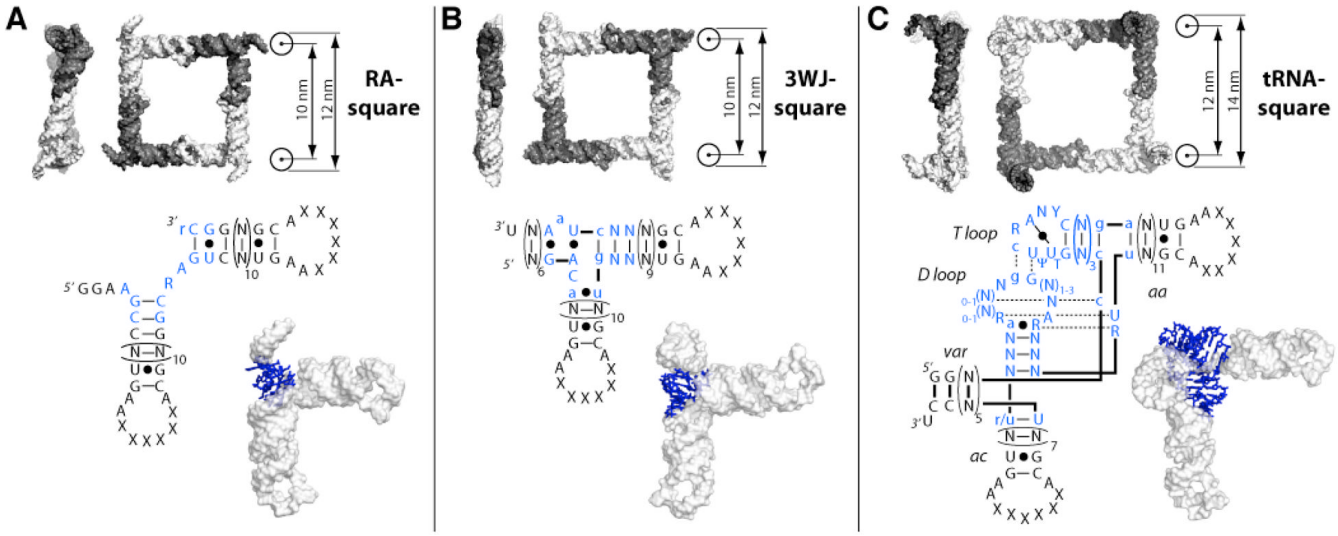

Figure 1.

90° motifs and corresponding tectoRNA and tectosquare structures. (Top) Front and side views of tectosquare models built from the RA- (A), 3WJ- (B) and tRNA- (C) motifs. (Middle and Bottom) Secondary and tertiary structures corresponding to L-shaped tectoRNAs. Each motif sequence signature is in blue. N, any nt; R, purine; Y, pyrimidine; X, nt positions involved in KL; Plain black bars, classic WC bps; Black circles or dashed lines, non-classic WC bps; Capital letters, conserved positions (> 95%); lower case letters, semi-conserved positions (>75%). For tRNA-tectoRNAs, *aa*, *ac* and *var* stand for amino-acyl, anticodon and variable stems, respectively. For 3WJ-P tectoRNAs, the 3WJ sequence signature (nt in blue) is rotated by 90° anticlockwise. Images were rendered in PyMol[36].

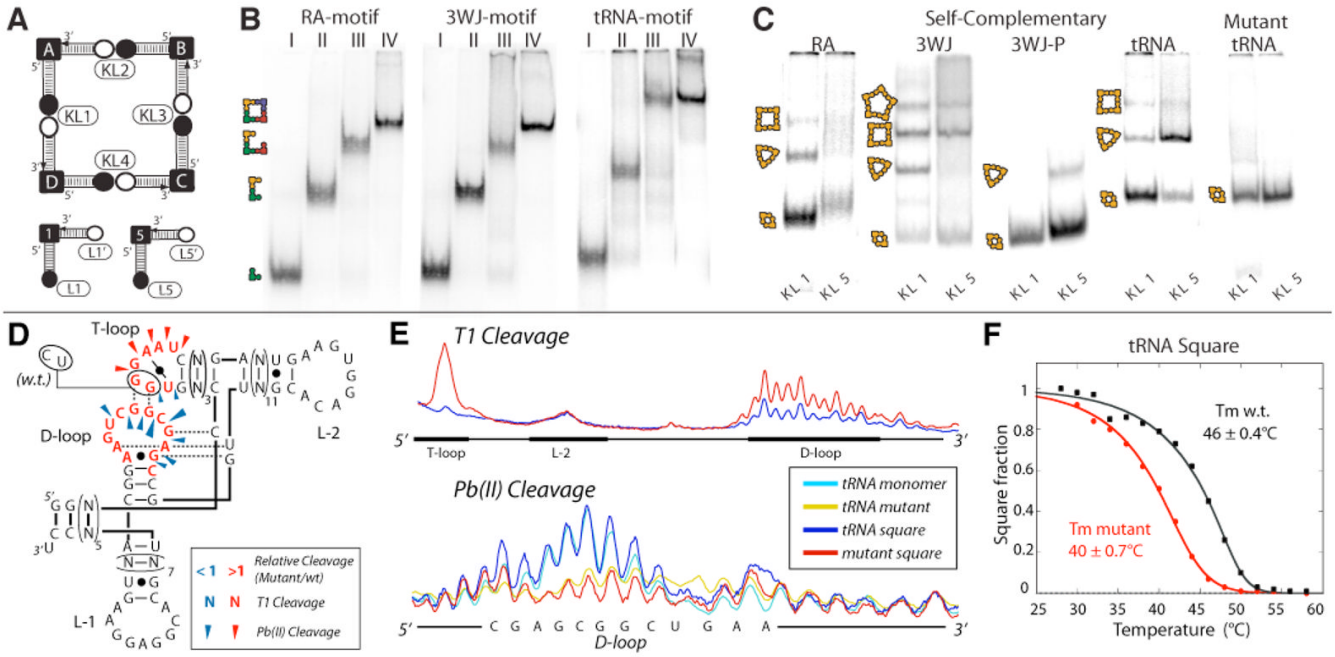

Figure 2.

Assembly scheme and native gel shift characterization of tectosquares incorporating different 90° motifs. (A) Each tectosquare is formed of 4 tectoRNAs (A,B,C and D) assembled through the same set of kissing loops (KL1-4). Self-complementary tectoRNAs (1 and 2) assemble through KL1 or KL5. (B) Native PAGE of various tectosquares (100 nM) assembled at 15 mM $Mg(OAc)_2$. I, monomer A; II, dimer AD; III, trimer ABC; IV, tetramer ABCD. (C) Assembly of self-complementary tectoRNAs (100 nM) into closed-NPs of various sizes at 15 mM Mg $(OAc)_2$. (D–F) The tRNA-square requires a folded tRNA motif for optimal assembly and stability. (D) Differential Pb^{2+} and RNase T1 cleavage patterns mapped on the secondary structure diagram of the mutated tRNA-square: Nt positions in red show enhanced T1 cleavage with respect of the w.t. (cleavage occurs 3′ of the nt). Phosphate positions that show enhanced or reduced Pb^{2+} cleavage with respect to the w.t. are indicated by red or blue arrows, respectively. (E) Examples of RNase T1 and Pb^{2+} cleavage profiles of various tRNA constructs at 15 mM $Mg(OAc)_2$. (F) Thermal melting curve of the tRNA-square with all four units mutated compared to the w.t.

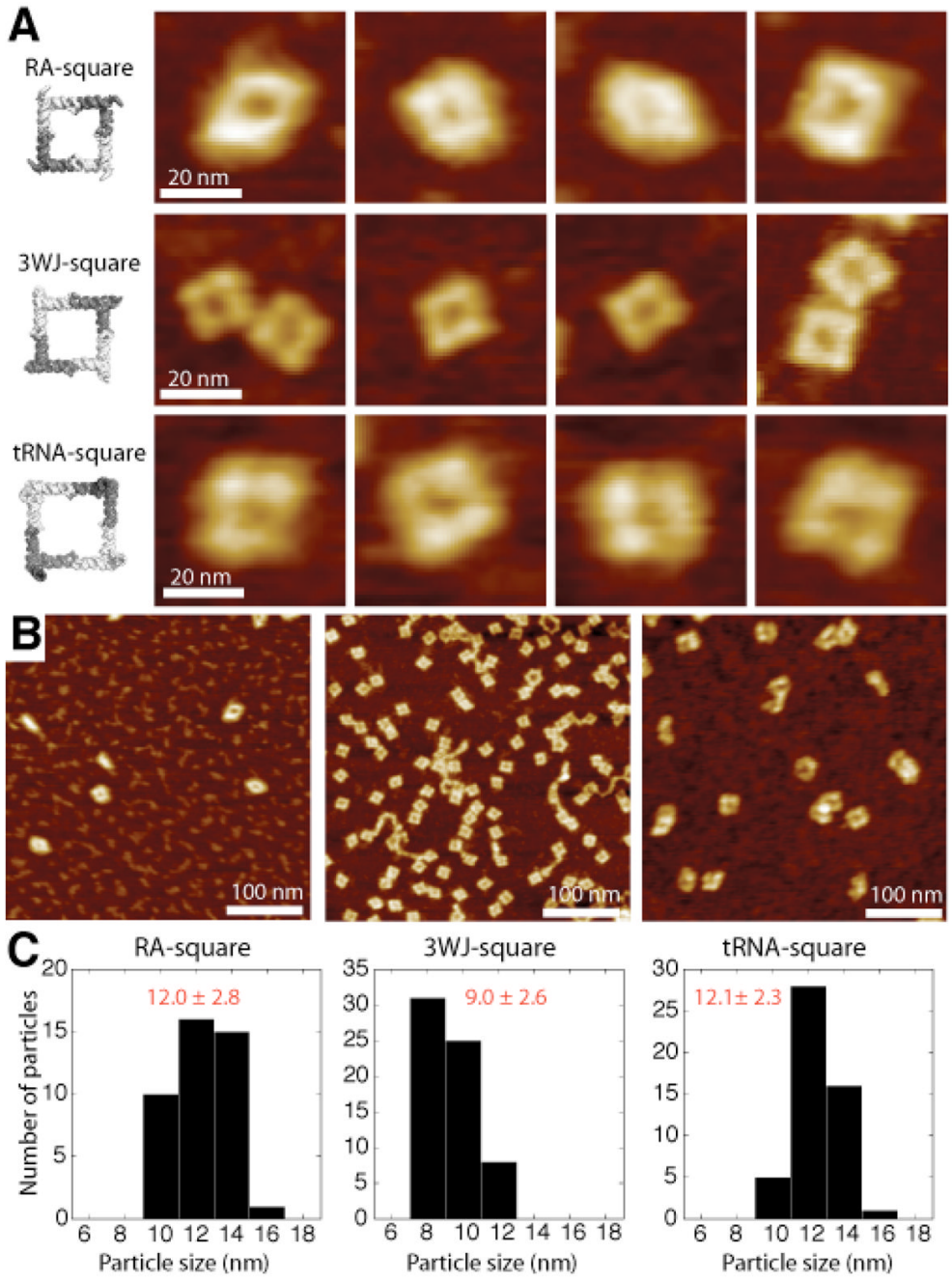

Figure 3.

AFM characterization of the RA-, 3WJ-and tRNA- squares. (A) Magnification of AFM images (scale bar 20 nm) for the RA-square (top), 3WJ-square (middle) and tRNA-square (bottom). (B) AFM images of the respective tectosquares (scale bar, 100 nm). Each image obtained in air corresponds to 100 nM solution of tectosquare deposited on freshly cleaved mica surface and dried. (C) Histograms showing the population distribution of NPs with respect to particle size.

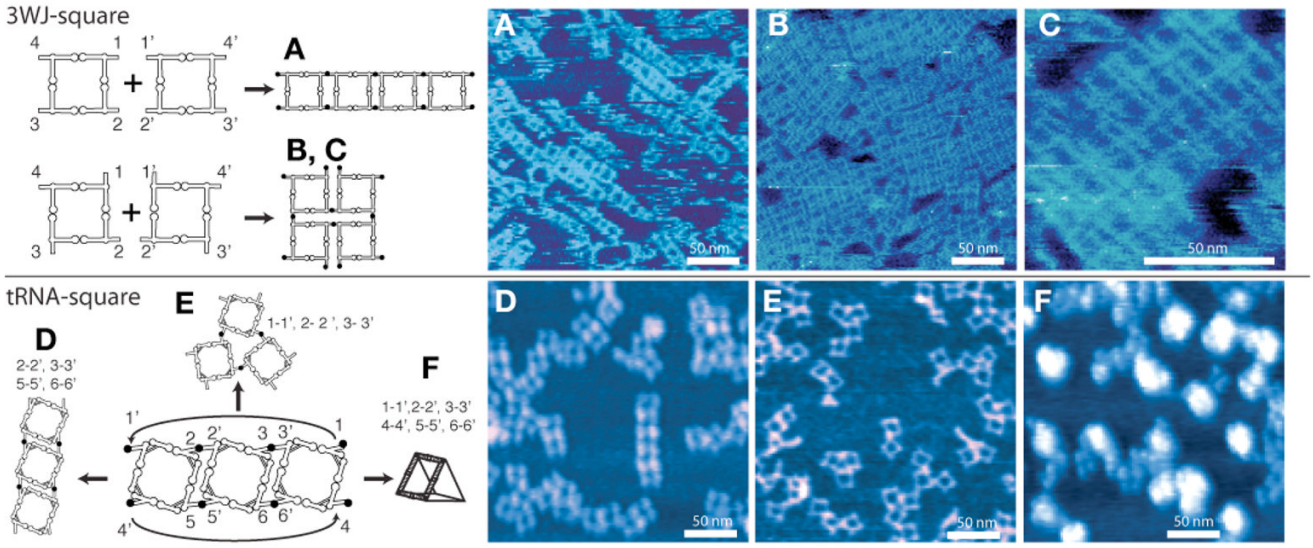

Figure 4.

Supramolecular assembly of 3WJ- and tRNA-squares. (Top) Assembly scheme and AFM images for 3WJ-square assemblies into ladders (A) and 2D arrays (B, C). (Bottom) Assembly scheme and AFM images for tRNA-square assemblies into finite sized ladders (D), triads (E) and 3D-prisms (F). The average height for the tRNA-ladders and triads is 1.5 nm. It is 3.4 ± 0.7 nm for 3D-prisms (see also Fig S8). All AFM images were obtained under 15mM $Mg(OAc)_2$. buffer solution as described [8].